Phase mask fabrication for multi-plane light conversion using grayscale lithography

SUDIP GURUNG,† SETH SMITH DRYDEN,† KEQI QIN AND GUIFANG LI

CREOL, College of Optics and Photonics, University of Central Florida, Orlando, 32816, USA
†These authors contributed equally.
**Sudip.gurung@ucf.edu*

Abstract: Direct writing laser (DWL) grayscale lithography is introduced as a novel fabrication technique for multi-plane light conversion (MPLC) phase masks, enabling direct transfer of precise depth profiles onto substrates via reactive ion etching and subsequent reflective coating. An MPLC system employing these masks achieves 92% fidelity in converting a Gaussian ($TEM_{0,0}$) input to a Laguerre-Gaussian ($LG_{0,15}$) mode. The fabricated masks exhibit sub-10 nm vertical resolution, surface roughness below 3 nm, and an R^2 value of 0.976. This method provides a scalable alternative to conventional multi-step lithographic fabrication for advanced photonic systems.

1. Introduction

Multi-plane light converters (MPLCs) are advanced optical devices that shape and transform light to high precision using a sequence of phase masks. MPLCs are used in a range of applications including beam shaping, beam combining, imaging, and communication applications such as mode (de)multiplexing (1-5). Because MPLCs consist only of phase multiplication and free-space propagation, they are theoretically inherently unitary and therefore lossless. In practice, some loss occurs due to small absorption at each reflection in the MPLC system, and imperfections in the beam shaping either through design limitations or fabrication defects. The phase masks for these devices are typically fabricated using lithographic techniques, where the optical path delay imparted by each pixel of the phase mask is twice the etch depth at that pixel (6). Typically, MPLC phase masks are fabricated using multi-layered binary etching, in which only a single lithographic depth is achieved per exposure. This means that traditional multi-layered binary lithography approaches require multiple rounds of exposure and etching. Fang et al. demonstrated an OAM multiplexing communication technique using inversely designed phase masks, which were fabricated using traditional lithography methods. Multiple rounds, at least 3 of UV lithography and dry etching were used to fabricate 8-step MPLC phase masks with a phase range from 0 to 2π (3). Achieving higher bit depth using this multi-exposure approach is both timely and difficult, as the wafer containing the masks must be carefully re-aligned after each sequence of exposure and etching before beginning the next layer's exposure. Failure to align the wafer correctly can introduce artefacts and defects into the phase masks that introduce various amounts of error and the scattering of a beam propagating through the MPLC system. Unlike traditional binary lithography, which creates discrete steps and is limited in achieving smooth phase profiles, grayscale lithography enables continuous height modulation across a substrate. This emerging technology represents a transformative approach to multi-layered etching, offering unprecedented control over phase modulation at the micro and nanoscale (7, 8). This capability allows for the creation of highly precise, complex phase masks that are essential for MPLC, where gradual and accurate phase control across multiple planes is critical for applications like mode sorting, beam shaping, and advanced optical interconnects. The continuous phase gradients achievable with grayscale lithography minimize aberrations and enhance the efficiency of mode conversion, enabling better light quality and intensity preservation across optical systems. Additionally, the flexibility of grayscale lithography supports the integration of intricate, multi-level phase profiles on a compact scale, making it an ideal choice for on-chip

photonic systems requiring compact, high-fidelity phase manipulation, fields such as quantum optics, biomedical imaging, and high-capacity optical communications, where precise light field control is a fundamental requirement.

While grayscale lithography effectively transfers 2.5D/3D designs onto photoresist, challenges remain, including proximity effect and nonlinear photoresist response to UV exposure, especially in creating complex topographies (9-11). Proximity effect is caused by light scattering and beam tails resulting in unintended exposures near the target in all lithography systems, are more detrimental to grayscale lithography because of their impact on the z-dimension (7). Mitigation of this effect requires careful design of the phase masks considering compensation for the edge placement error (EPE) and consideration of critical dimension (CD) (12-14). Of greater significance is the nonlinear relationship, frequently termed the "contrast curve," which exhibits a disproportionate correlation between photoresist thickness/profile and fluctuations in exposure intensity or grayscale level (15). Despite a linear exposure-response curve, various factors including bleaching effects from UV exposure, developer chemistry variability, photoresist inconsistencies, and pre- and post-baking parameters can induce substantial nonlinearities. This challenge was mitigated via optimization of the iterative grayscale value distribution (GVD) technique and proximity effect correction (PEC), a method previously validated by Erjawetz et al. (9). In this approach, a test pattern is exposed and developed, then the depth is measured. Any deviation from the target profile is fixed by modifying the grayscale distribution with custom-coded recalibration software. This iterative process of exposing, measuring, and adjusting continues until the final topography conforms to the specified design. This approach, in its present form, is problematic because it requires multiple manufacturing steps and recalibration of the grayscale distribution. Recently, Chen et al. used a digital micro mirror (DMD) based grayscale lithography system (Heidelberg MLA 100 Mask Aligner) to fabricate a 6-bit phase mask for mode-division multiplexing (MDM) (5). This manufacturing method, however, suffers from several drawbacks: resolution below 1 μm is difficult to achieve, exposure is discrete, and stitching artifacts are present; hence, it is not ideal for photonic devices. Moreover, attaining higher-bit grayscale values presents a considerable challenge owing to the intrinsic limitations of DMDs. These devices modulate amplitude via pulse-width modulation; each micromirror is either active or inactive, with grayscale intensity determined by the micromirror's on-time proportion. The mirror switching speeds and data throughput of DMD-based grayscale lithography are hardware-constrained, limiting higher bit-depth (gray scale) operation. Moreover, the device resolution is substantially affected by DMD pixel dimensions, thereby restricting pixel size. The production of these phase masks involved etching photoresists and applying a gold reflective layer; this process, however, compromises their durability and application versatility. We have not encountered any published reports of phase masks created through the etching of grayscale lithographic patterns onto a substrate. Alternatively, grayscale in a direct writing laser (DWL) system is achieved by modulating laser intensity with an acousto-optic modulator (AOM) and is further refined by adjusting scanning speed and dwell time (7). Pixel size is not limited as it is in DMD grayscale lithography; instead, the limit here is the diffraction-limited spot size of the beam, determined by numerical aperture, wavelength, and scanning precision (16). In addition, the use of Heidelberg DWL 66+ grayscale lithography can provide up to 16-bit grayscale levels. Despite their versatility in transferring designs onto resist structures, laser-based pattern generators face challenges with non-linear responses, proximity effects from laser-photoresist interactions, especially when creating sloped, stepped, or continuous topographies (11).

In this work, we present the first demonstration of phase masks etched into a substrate using grayscale lithography for multi-plane light conversion (MPLC) devices. Unlike conventional multi-step lithographic techniques requiring complex processing for precise phase profiles, our approach uses direct writing laser (DWL) grayscale lithography to directly pattern depth profiles onto a photoresist, followed by reactive ion etching (RIE) and a reflective coating. This

method enables high-fidelity phase mask fabrication with improved precision and scalability. To validate our approach, we construct an MPLC system that converts an input Gaussian mode ($TEM_{0,0}$) into an output Laguerre-Gaussian ($LG_{0,15}$) mode, achieving a 92% fidelity of the output mode. Depth profile analysis of the masks shows an R^2 value of 0.976 and a surface roughness (Sa) below 3 nm, confirming the accuracy of the grayscale lithographic patterning and etching process. Furthermore, this lithographic method shows near-unity selectivity, and sub-10 nm vertical resolution, establishing grayscale lithography as a robust and scalable technique for fabricating high-precision MPLC phase masks directly into substrates.

2. Phase Mask Design and MPLC System Configuration

Multi-Plane Light Conversion (MPLC) devices use a series of phase masks to transform a set of orthogonal input light distributions into a corresponding set of orthogonal output distributions via unitary transformations. Designing phase masks for MPLC systems is a highly non-convex process, resulting in numerous local minima and solutions mapping inputs to outputs. The inherent non-convexity of the inverse design problem for MPLC phase masks necessitates the use of parametric sweeps to explore various solutions when using deterministic methods. A common way to handle non-convex problems is through the use of stochastic gradient descent (17). We adapt this approach, or parts of it, to create MPLC phase mask designs. For instance, our method randomly chooses at each iteration whether to update masks during the forward pass, the backward pass, or both. We also generate the phase masks by calculating a weighted sum of the mode mappings, with random weights. This new method introduces stochastic elements into the design process; it successfully functions as stochastic gradient descent in convex optimization and as a randomized perturbation in the wavefront matching algorithm. Since our method produces varying designs in each iteration, we repeat the process until we achieve the desired performance.

An MPLC system, illustrated in Figure 1, is a single pass cavity that transforms an input beam (e.g., a Gaussian beam) into a desired output using a sequence of 4 phase masks. The phase of the beam is altered at each mask location, which then couples into amplitude changes through free-space diffraction between each mask (i.e., Fourier coupling). The phase masks for an MPLC can either be displayed digitally using an SLM, or etched into a phase mask, as shown in Figure 1(a). The advantage of the former is that the MPLC can be controlled actively, while the latter allows for unity pixel fill-factor, higher reflectivity of the masks, and smaller pixel sizes, giving greater beam control and higher efficiency. The design process for the phase masks involves a non-convex free-space inverse design problem, typically solved using forward-backward algorithms such as wavefront matching [will add citation] or optimization methods like gradient descent with initialization. For our application, we designed an MPLC system for a Gaussian input at $\lambda = 1630$ nm, entering the system 2 cm from the first mask. The mirror, illustrated in Figure 1(a), is positioned 12 mm from the phase mask, and the output distribution, an $LG_{0,15}$ mode, is designed such that the beam waist aligns with the mirror (i.e., 12 mm after the final phase mask). While the input beam is coupled at an angle of 7.125° relative to the normal axis of the phase mask. The MPLC consists of four masks, each containing 600 x 600 pixels, with a pixel size of 5 μm. Figure 1(b) illustrates a mode conversion mechanism employing multiple phase masks to transform a Gaussian ($TEM_{0,0}$) input mode into a Laguerre-Gaussian ($LG_{0,15}$) output mode. To illustrate the mode conversion process, the beam's state immediately following each phase mask is depicted.

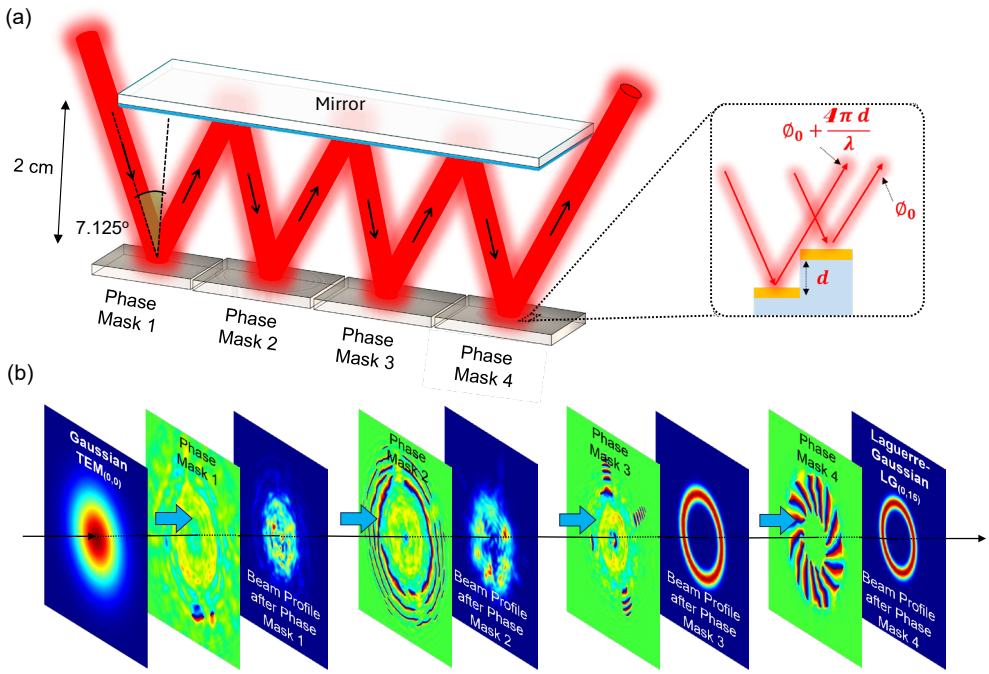

Figure 1: Laguerre-Gaussian beam conversion on multi-plane beam conversion. (a) Representation of reflective type MPLC mode conversion using phase masks and mirror. Inset: working mechanism of phase masks, i.e., phase manipulation via path length difference. (b) Mode conversion mechanism using multiple phase masks for the transformation of Gaussian ($TEM_{0,0}$) to Laguerre-Gaussian ($LG_{0,15}$) output mode.

3. Direct writing laser Grayscale Lithography for MPLC Phase Mask Fabrication

Grayscale lithography is an advanced fabrication technique used to create micro- and nanostructures with varying depths and complex geometries (7, 16, 18-20). While conventional binary photolithography has evolved to enable curved mask layer fabrication in the x- and y-dimensions, grayscale lithography extends this capability into the z-dimension, allowing for the generation of continuously variable structures. This distinguishes grayscale lithography from traditional lithographic techniques, which are limited to binary patterning. In this study, phase masks were fabricated using Heidelberg Direct writing laser (DWL 66+) grayscale lithography. The system offers different writing speed modes, with a critical dimension (CD) in the x-y plane ranging from 0.6 µm to 2 µm. For this application, a fast-writing mode was selected, operating at 600 mm²/min with a minimum structure size of 1 µm, making it well-suited for phase masks with a pixel size of 5 µm. The schematic representation of the phase mask manufacturing process, which integrates the photoresist chemistry, DWL grayscale lithography, reactive ion etching (RIE) for pattern transfer and reflective coating is depicted in Figure 2. During the lithography process, a photoresist layer (ma-P 1215) is exposed to UV light at 405 nm, with spatially modulated intensity controlling photon absorption within the resist. Upon UV exposure, the dissolution rate of the exposed photoresist in aqueous-alkaline developers increases significantly, while the unexposed resist exhibits a minimal but non-zero dissolution rate. The dissolution rate increases proportionally with exposure dose, resulting in a gradual reduction of resist film thickness after development. Utilizing ma-D 533S photoresist developer, a specialized formulation for ma-P 1215 grayscale photoresist, ensures precise exposure and height control during sample development. The photoresist and developer are commercially available products manufactured by micro resist technology GmbH (15).

Following development, the surface depth profile of the photoresist was etched into the silicon substrate using reactive ion etching.

A key challenge in grayscale lithography is the accurate replication of depth profiles from photoresist to substrate. For this purpose, RIE has demonstrated superior efficacy due to its capacity for precise selectivity control through manipulation of its parameters (21). Lima et al. demonstrated that a three-dimensional photoresist pattern could be transferred onto a silicon substrate with 50 nm z-depth precision, achieving both unity selectivity and anisotropy (19). Similarly, Gerges et al. explored the use of low-contrast resist (ma-P1225G) to enhance step height control, investigating the effects of soft bake and post-exposure bake on resist profiles (22). They employed HBr based inductively coupled plasma (ICP) etching process to achieve a step height resolution of 20 nm in the photoresist and 50 nm in silicon. This work employed an Oxford Plasma Pro ICP-RIE system for pattern transfer, utilizing an $SF_6/C_4F_8/O_2$ plasma-based etching process optimized to achieve near-unity etch selectivity. The resultant process demonstrated precise depth control, achieving unity selectivity. Notably, a single RIE process enabled the etching of up to 256 distinct depth levels onto a silicon wafer. To complete the phase mask fabrication, a thin (45 nm) aluminum reflective coating was applied using a Temescal FC-2000 electron beam evaporation machine. A critical challenge in deploying metallic reflector coatings and mirrors is the reduction in intermodal power conversion efficiency. Losses can become substantial with a growing number of phase masks, as each reflection may individually induce losses exceeding 3%. Nevertheless, this can be mitigated with the utilization of low-loss dielectric mirrors and coatings. Despite its versatility in transferring designs into resist structures, laser-based pattern generators present certain challenges, including non-linear responses and proximity effects caused by laser-photoresist interactions (7, 9, 23-26). Additionally, different topographies, such as sloped, stepped, or continuous structures, pose varying levels of fabrication complexity. Addressing these challenges is crucial for achieving precise and reproducible grayscale lithographic patterns (11).

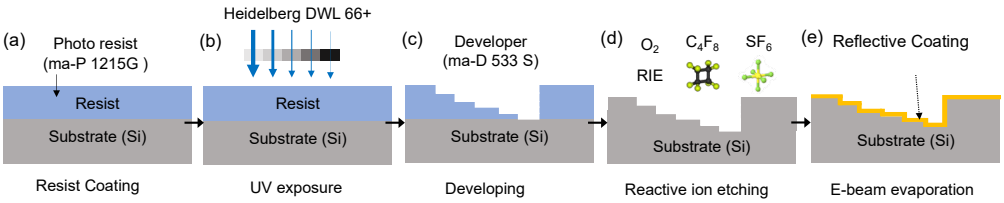

Figure 2 (a-e): Schematic illustration of the steps involved in the phase mask fabrication process.

A significant challenge in grayscale lithography is the nonlinear relationship between developed resist depth and grayscale levels, stemming from the photoresist's response to exposure dose (*7, 10, 15, 18, 20*). Accurate depth reproduction in grayscale lithography critically depends on a linear ultraviolet response. A comprehensive analysis of ma-P 1215 from Micro-Resist technologies, a high-quality photoresist, has recently been published (15). Utilization of this photoresist has significantly shortened the optimization phase and enabled the fabrication of high-quality phase masks. Analysis of a 1.5 µm thick ma-P 1215 photoresist exposed to varying grayscale values revealed a linear correlation ($y = -6.53 - 3.16x$), depicted in Figure 3. The similarity between the expected (3.17) and fitted (3.16) slopes support the photoresist's linear behavior. Several factors contribute to this effect. Thicker photoresists absorb more light near the surface, causing uneven exposure with depth, while thinner resists provide more uniform dose distribution. Additionally, thicker resists produce stronger standing-wave interference patterns at normal incidence, leading to pronounced intensity variations

resulting in non-uniform developed depths (*27*). Reduced thickness mitigates these interference effects, resulting in more uniform development.

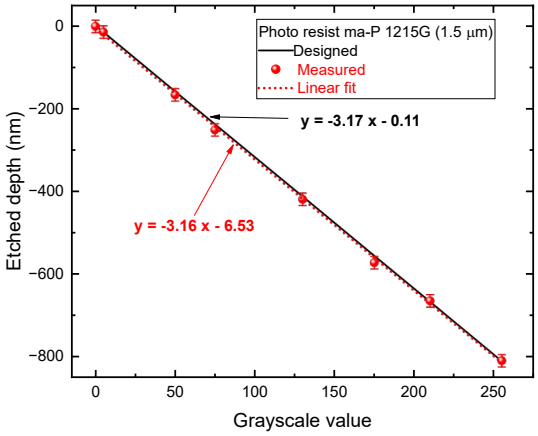

Figure 2: Linear behavior of thin photoresist (ma-P 1215), 1.5 μm thick photo resist was exposed to different grayscale, the sample was then developed and etched into the silicon substrate.

An enlarged pixel size of 5 μm has been implemented to reduce the proximity effect. Increased pixel size reduces overlapping exposures, thus minimizing unintended exposure to neighboring pixels. Averaged exposures are obtained by utilizing multiple lower-dose beam exposures to compensate for bleaching and non-uniform exposures within each pixel. Furthermore, employing a thinner photoresist mitigates proximity effects through scattering reduction, enhances resolution by diminishing standing wave interference and optical path lengths, ensures a more uniform dose distribution via improved exposure consistency, and allows for more precise aspect ratio control through predictable development. Consequently, optimization of the grayscale lithography process, along with the appropriate selection and thickness of photoresist, is critical for the fabrication of high-quality phase masks.

4. Experimental characterization and validation of device performance

To validate the accuracy of the fabricated phase mask, an eight-bar staircase structure was incorporated into each mask, as illustrated in Figure 4 (a). Each bar measured 30 μm in width, with ` depth corresponding to grayscale levels of 0, 5, 25, 50, 130, 175, 210, and 255. To mitigate any potential bias introduced during fabrication, the grayscale values used were selected randomly. Also, the grayscale value of 130 is considered as the origin as shown in Figure 4 (b and c) representing height of 0 nm, 16 nm, 159 nm, 238 nm, 412 nm, 555 nm, 666 nm, and 809 nm were etched between each mask. These bars serve as quality control indicators. Analysis with a Bruker Dektak XT surface Profilometer (15 nm measurement error) and a Keyence VK-X3000 optical Profilometer (sub-10 nm measurement error) revealed a strong similarity between the designed and actual depths, confirming the high quality of the fabricated phase masks Figure 4 (b). The staircase bar areas in Figure 4 (c), regions A and B, demonstrated exceptionally low surface roughness (Sa), measuring below 3 nm, which are tabulated in Figure 4 (d). The measured maximum depth of the staircase bars (810 nm) is consistent with the design specification $\left(809 \text{ nm} \approx \frac{1630 \times cos(7.125^0)}{2}\right)$ within the Profilometer's measurement uncertainty (see Figure 4 (d)). Discrepancies in height measurements between mechanical and optical Profilometer arise from the fundamental difference in their measurement principles. Mechanical Profilometer employs a physical stylus for direct surface contact, thus obtaining a direct representation of topography. However, this method is inherently limited by stylus tip dimensions and the potential for surface deformation. Conversely, non-contact optical Profilometer determines surface profiles via confocal laser scanning, achieving both high

resolution and speed, yet their performance is susceptible to optical characteristics and environmental factors. These two measurement techniques were implemented to independently ensure accuracy of measurement.

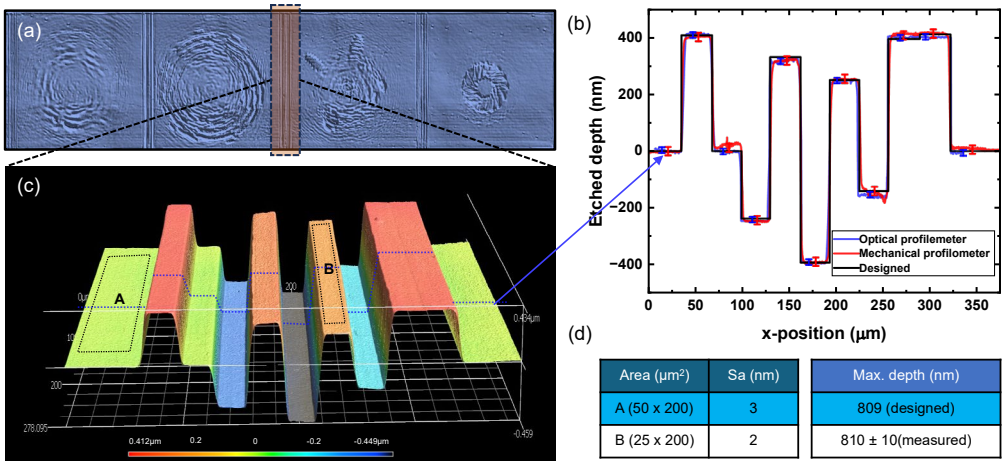

Area (µm²)	Sa (nm)	Max. depth (nm)
A (50 x 200)	3	809 (designed)
B (25 x 200)	2	810 ± 10(measured)

Figure 3: (a) Low resolution optical Profilometer image of the entire phase masks showing four individual phase masks with eight-bar staircase structure in between. (b) Comparison of design and actual depth measured using optical and mechanical Profilometer. Each of the height bars includes an error bar for the different measurement techniques. (c) Optical Profilometer image of quality control indicators with different designed height, each 30 µm width. (d) Table of the surface roughness for arithmetic mean height (Sa) at the designated area A and B as shown in Figure 4(a).

Quantitative assessment of the similarity between the designed and measured depths was performed using statistical methods (R^2 calculation). The R^2 value lies in between 0 to 1, with 0 indicating total disparity and 1 signifying perfect congruence between target and measured values. R^2 calculation was conducted using (*28*)

$$R^2 = 1 - \frac{\Sigma(Z_{measured} - Z_{designed})^2}{\Sigma(Z_{measured} - Z_{measured\,mean})^2} \quad (1)$$

where, $Z_{measured}, Z_{designed}, and\ Z_{measured\,mean}$ are the measured, designed and arithematic mean of the measured heights with in a bar. $Z_{measured}$ from Figure 4 (b) was used for the R^2 calculation. Previously, a value of 0.842 was reported for a staircase using an optimization method (9), in which the nonlinearity of the photoresist was calibrated and compensated by adjusting the exposure time (16). Moreover, using the proximity exposure correction (PEC) and gray value distribution (GVD) iterative correction technique, the R^2 values were further improved to 0.998 and 0.994 respectively (9). The fabricated staircase bars as shown in Figure 4(b) show R^2 values of 0.939 (mechanically measured z-depth) and 0.976 (optically measured z-depth). These values are comparable with the PEC and GVD iterative corrective technique. Getting the desired z-depth control using the DWL grayscale lithography depends on a multitude of factors such as grayscale exposure, photoresist development, substrate etching, and reflective metallization. Careful optimization of thin grayscale photoresist, unity selectivity in reactive ion etching, and ultra-flat 45 nm aluminum e-beam evaporation yielded a high-quality phase mask, eliminating complex optimization steps.

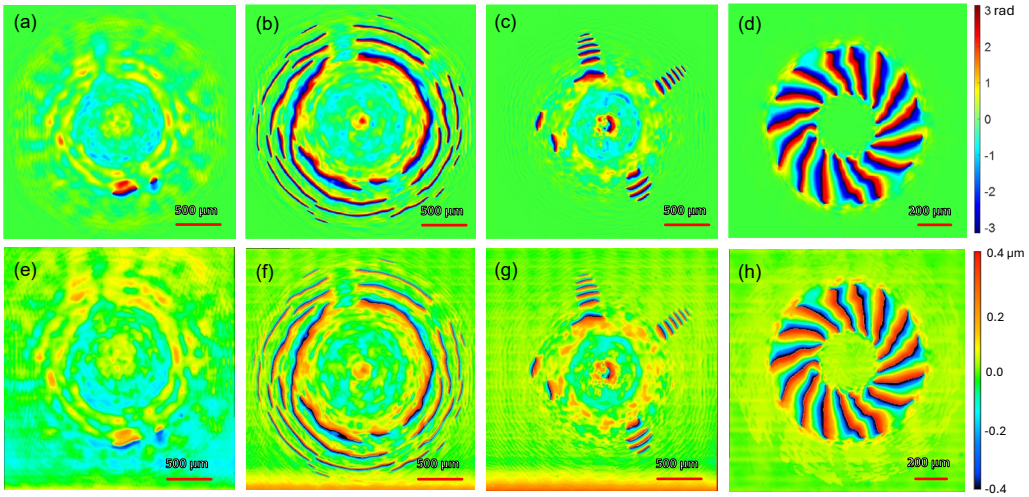

Figure 4: Optimized phase mask for converting fundamental Gaussian ($TEM_{0,0}$) to Laguerre-Gaussian ($LG_{0,15}$) beam at 1630 nm. Here, a, b, c, and d are simulated phase masks, whereas e, f, g, and h are the fabricated phase masks. Three-dimensional surface profiles of the phase masks are obtained using a Keyence VK-X3000 optical Profilometer.

Figure 5 show simulated and fabricated Gaussian ($TEM_{0,0}$) to Laguerre-Gaussian ($LG_{0,15}$) mode conversion phase masks. The simulated phase masks shown in Figure 5(a–d) correspond to the fabricated phase masks in Figure 5 (e–h), where the phase-to-path length relationship is given by $\Delta\emptyset = 4\pi d/\lambda$. Here, $\Delta\emptyset$ denotes the phase shift and d represents the corresponding optical path length. Minor inconsistencies in the fabricated phase mask may be attributed to limitations inherent in the optical Profilometer measurement methodology, which involves stitching together 150 individually scanned high resolution surface profile maps to produce a single composite image of a single-phase mask. Given the inherent complexities of the measurement process, a direct comparison of the simulated and fabricated phase masks was not performed.

Alternatively, the comparative analysis of these phase masks is rigorously conducted by evaluating their mode conversion capabilities, experimentally validated in Figure 6. The process involved interfering a Gaussian ($TEM_{0,0}$) mode with a converted Laguerre-Gaussian ($LG_{0,15}$) mode to create an interferogram (see Figure 6 (a)). A quantitative analysis of the agreement between simulated and experimental interferograms was conducted, employing a fidelity metric (F) on their intensity distributions. The fidelity (F) is calculated as:

$$F = \left(\iint \sqrt{\frac{I_{\mathrm{sim}}(x,y)}{\iint I_{\mathrm{sim}}(x,y)\,dx\,dy} \cdot \frac{I_{\mathrm{exp}}(x,y)}{\iint I_{\mathrm{exp}}(x,y)\,dx\,dy}}\, dx\,dy \right)^2 \times 100\ \% \qquad (2)$$

Where, $I_{sim}(x,y)$ and $I_{exp}(x,y)$ represent the simulated and experimentally obtained interferogram intensities, respectively. This metric quantifies the degree of overlap between the two intensity patterns, thus representing their similarity. Strong agreement is evident in both fringe structure and spatial intensity distribution; with the 92% fidelity between simulated and experimental interferograms, validating the mode purity of the converted Laguerre-Gaussian ($LG_{0,15}$) mode. A lens was introduced to ensure the reference and converted beams exhibited identical dimensions at the imaging plane. The appearance of curved circular fringes in both simulation and experiment, as seen in Figure 6 (b and c), arises from the quadratic phase modulation imparted by a lens placed along the path of the reference Gaussian beam. The presence of secondary fringe patterns adjacent to the primary circular interference fringes is attributable to reflections or scattering from ancillary optical elements within the system.

Although exhibiting high fidelity, minor inconsistencies may result from a variety of factors. One contributing factor might be the non-unity R^2 value observed in the fabricated sample; this could potentially be addressed through optimization in grayscale lithography process. A significant contributing factor is scattering losses, primarily resulting from the sharply defined pixels of the phase masks. This problem can be resolved through a smooth transition, such as the absence of a significant step height between pixels while designing the phase masks. MPLC phase masks produced via DWL grayscale lithography exhibited exceptional performance, generating highly promising results. With modest process optimization, commercial implementation of this method in phase mask production is feasible.

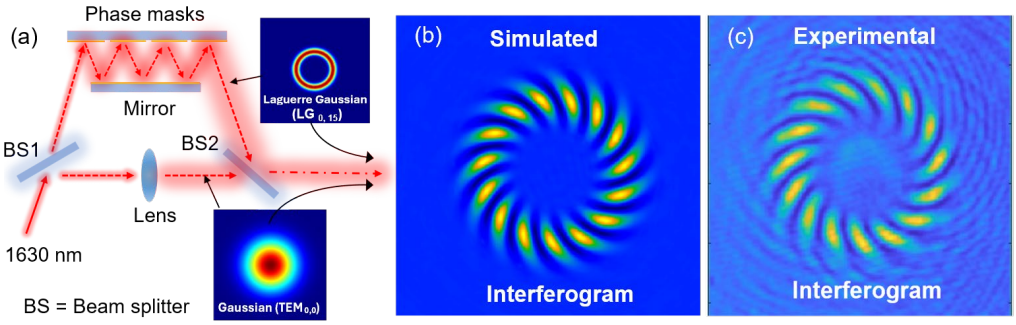

Figure 5: (a) Experimental demonstration of fidelity using interferogram. An illustration of the Gaussian ($TEM_{0,\ 0}$) and Laguerre-Gaussian ($LG_{0,\ 15}$) modes interfering to produce (b) the simulated and (c) experimental interferograms.

5. Conclusion

A novel direct writing laser (DWL) grayscale lithography technique, combined with reactive ion etching (RIE), has been successfully employed in this work to fabricate high-precision phase masks for multi-plane light conversion (MPLC) devices. The DWL method offers a significant simplification of the fabrication process through the direct patterning of accurate depth profiles on substrates, eliminating the constraints associated with traditional multi-step lithographic approaches. A fidelity of 92% was attained in the conversion of an input Gaussian ($TEM_{0,0}$) mode to a Laguerre-Gaussian ($LG_{0,15}$) mode, thus confirming the enhanced precision and robustness of our approach. The phase masks exhibited exceptional accuracy in their comprehensive characterization, achieving an R^2 value of 0.976 and a remarkably low surface roughness (Sa) of less than 3 nm. Results from grayscale lithography show exceptional properties—near-unity selectivity, and sub-10 nm vertical resolution showing its suitability for high-performance, scalable MPLC applications. While this study represents substantial advancement, future research will fully realize the potential of grayscale lithography through optimization of continuously engineered depth profiles for continuous phase modulation. Attainment of this goal enables a higher degree of phase modulation precision, resulting in considerable enhancement of MPLC system performance and versatility. The achievement of optimized continuous depth profiles is expected to greatly enhance the utility of MPLC devices in state-of-the-art photonic and optical communication technologies.

Acknowledgements

The authors acknowledge the financial support provided by the Office of Naval Research (ONR), grant number N6833524C0357, for the research undertaken at CREOL, College of Optics and Photonics, University of Central Florida. Acknowledgment is given to the Interdisciplinary Research and Incubator Facility (IRIF), Research I Building Cleanroom, for its assistance with grayscale lithography fabrication. SG and SS contributed equally to this work.

Disclosures. The authors declare no conflicts of interest.

References:

1. X. Chen, X. Yan, J. Fang, T. Lei, F. Pang, Multi-plane light conversion (MPLC) LP mode multiplexer based on grayscale maskless lithography. *Optics Express* **32**, 40305-40314 (2024).
2. N. K. Fontaine *et al.*, in *2022 European Conference on Optical Communication (ECOC)*. (IEEE, 2022), pp. 1-4.
3. J. Fang *et al.*, Optical orbital angular momentum multiplexing communication via inversely-designed multiphase plane light conversion. *Photonics Research* **10**, 2015-2023 (2022).
4. N. K. Fontaine *et al.*, Laguerre-Gaussian mode sorter. *Nature communications* **10**, 1865 (2019).
5. Z. Zhu, J. H. Doerr, G. Li, S. Pang, in *Digital Holography and Three-Dimensional Imaging*. (Optica Publishing Group, 2022), pp. M6A. 2.
6. Y. Zhang, Multi-Plane Light Conversion: a Practical Tutorial. *arXiv preprint arXiv:2304.11323*, (2023).
7. S. N. Khonina, N. L. Kazanskiy, M. A. Butt, Grayscale Lithography and a Brief Introduction to Other Widely Used Lithographic Methods: A State-of-the-Art Review. *Micromachines* **15**, 1321 (2024).
8. C. Waits, B. Morgan, M. Kastantin, R. Ghodssi, Microfabrication of 3D silicon MEMS structures using gray-scale lithography and deep reactive ion etching. *Sensors and Actuators A: Physical* **119**, 245-253 (2005).
9. J. Erjawetz *et al.*, Bend the curve–shape optimization in laser grayscale direct write lithography using a single figure of merit. *Micro and Nano Engineering* **15**, 100137 (2022).
10. I. Khazi, U. Muthiah, U. Mescheder, 3D free forms in c-Si via grayscale lithography and RIE. *Microelectronic Engineering* **193**, 34-40 (2018).
11. A. Grushina, Direct-write grayscale lithography. *Advanced Optical Technologies* **8**, 163-169 (2019).
12. C. A. Mack, in *Optical Microlithography IX*. (SPIE, 1996), vol. 2726, pp. 634-639.
13. J.-Y. Hur, M.-S. Seo, Optical proximity corrections for digital micromirror device-based maskless lithography. *Journal of the Optical Society of Korea* **16**, 221-227 (2012).
14. C.-L. Weng, C.-Y. Wu, Y.-C. Lee, Enhanced corner sharpness in DMD-based scanning maskless lithography using optical proximity correction and genetic algorithm. *Optics Express* **32**, 45357-45372 (2024).
15. C. Schuster *et al.*, Advancing greyscale lithography and pattern transfer of 2.5 D structures using ma-P 1200G resist series. (2022).
16. Q. Deng *et al.*, Fabrication of micro-optics elements with arbitrary surface profiles based on one-step maskless grayscale lithography. *Micromachines* **8**, 314 (2017).
17. X. Sui, Z. He, D. Chu, L. Cao, Non-convex optimization for inverse problem solving in computer-generated holography. *Light: Science & Applications* **13**, 158 (2024).
18. Y. Pang *et al.*, 3D stretchable arch ribbon array fabricated via grayscale lithography. *Scientific Reports* **6**, 28552 (2016).
19. F. Lima, I. Khazi, U. Mescheder, A. C. Tungal, U. Muthiah, Fabrication of 3D microstructures using grayscale lithography. *Advanced Optical Technologies* **8**, 181-193 (2019).
20. K. Totsu, K. Fujishiro, S. Tanaka, M. Esashi, Fabrication of three-dimensional microstructure using maskless gray-scale lithography. *Sensors and Actuators A: Physical* **130**, 387-392 (2006).

21. K.-C. Chien, C.-H. Chang, Controlling the etch selectivity of silicon using low-RF power HBr reactive ion etching. *Journal of Vacuum Science & Technology B* **40**, (2022).
22. N. Gerges *et al.*, Optimized ultraviolet grayscale process for high vertical resolution applied to spectral imagers. *Journal of Vacuum Science & Technology B* **39**, (2021).
23. M. Meunier *et al.*, in *Proceedings of ICALEO*. (2019).
24. C. R. Ocier *et al.*, Direct laser writing of volumetric gradient index lenses and waveguides. *Light: Science & Applications* **9**, 196 (2020).
25. X. Wang *et al.*, Femtosecond laser-based processing methods and their applications in optical device manufacturing: A review. *Optics & Laser Technology* **135**, 106687 (2021).
26. C. Zenz *et al.*, Simulation-based process optimization of laser-based powder bed fusion by means of beam shaping. *Additive Manufacturing* **77**, 103793 (2023).
27. T. A. Brunner, in *Advances in Resist Technology and Processing VIII*. (SPIE, 1991), vol. 1466, pp. 297-308.
28. A. C. Cameron, F. A. Windmeijer, An R-squared measure of goodness of fit for some common nonlinear regression models. *Journal of econometrics* **77**, 329-342 (1997).